Journal of the Korean Astronomical Society
48: 365 ∼ 380, 2015 December
©2015. The Korean Astronomical Society. All rights reserved.
http://dx.doi.org/10.5303/JKAS.2015.48.6.365
pISSN: 1225-4614 · eISSN: 2288-890X
http://jkas.kas.org

Molecular Outflows from Newly Formed Massive Stars

Kee-Tae Kim[1], Won-Ju Kim[1,2], and Chang-Hee Kim[1,3]

[1]Korea Astronomy and Space Science Institute, 776 Daedeok-daero, Yuseong-gu, Daejeon 34055, Korea; ktkim@kasi.re.kr
[2]Max-Planck-Institut für Radioastronomie, Auf dem Hügel 69, 53121, Bonn, Germany
[3]Department of Physics and Astronomy, FPRD, Seoul National University, Seoul 151742, Korea

Received November 20, 2015; accepted December 13, 2015

Abstract: We map 6 massive young stellar objects (YSOs) in the CO J=2–1 line and survey 18 massive YSOs, including the six, in the HCO^+ J=1−0, SiO J=2−1, H_2O $6_{16} - 5_{23}$ maser, and CH_3OH $7_0 - 6_1$ A^+ maser lines. We detect CO bipolar outflows in all the six mapped sources. Four of them are newly discovered (07299−1651, 21306+5540, 22308+5812, 23133+6050), while 05490+2658 is mapped in the CO J=2–1 line for the first time. The detected outflows are much more massive and energetic than outflows from low-mass YSOs with masses >20 $M_\odot$ and momenta >300 $M_\odot$ km s^{-1}. They have mass outflow rates (3−6)×10^{-4} $M_\odot$ yr^{-1}, which are at least one order of magnitude greater than those observed in low-mass YSOs. We detect HCO^+ and SiO line emission in 18 (100%) and 4 (22%) sources, respectively. The HCO^+ spectra show high-velocity wings in 11 (61%) sources. We detect H_2O maser emission in 13 (72%) sources and 44 GHz CH_3OH maser emission in 8 (44%) sources. Of the detected sources, 5 H_2O and 6 CH_3OH maser sources are new discoveries. 20081+3122 shows high-velocity (>30 km s^{-1}) H_2O maser lines. We find good correlations of the bolometric luminosity of the central (proto)star with the mechanical force, mechanical luminosity, and mass outflow rate of molecular outflow in the bolometric luminosity range of 10^{-1}−10^6 $L_\odot$, and identified 3 intermediate- or high-mass counterparts of Class O objects.

Key words: ISM: jets and outflows — ISM: molecules — masers — stars: formation — stars: protostars

1. Introduction

It has been well established since the mid 1980's that bipolar molecular outflows are an important component in the formation process of low-mass stars (see Bachiller 1996 and references therein). While studies on outflows associated with massive young stellar objects (YSOs) have a much shorter history, they may also be ubiquitous (e.g., Shepherd & Churchwell 1996a; Osterloh et al. 1997; Zhang et al. 2001; Sridharan et al. 2002). For example, Shepherd & Churchwell (1996) made an extensive CO J=1−0 line survey towards 122 massive YSOs and found high-velocity wings in about 90%. Zhang et al. (2001) and Sridharan et al. (2002) also obtained similar detection rates for smaller (69 and 39 sources) samples. Taking into account the close relationship between accretion and outflow processes, these observations strongly suggest that accretion may play an important role in the formation process of massive stars as in low-mass star formation. Bipolar outflows from massive YSOs seem to have much larger opening angle (>50°), mass (>10 $M_\odot$), and mechanical luminosities than those observed in low-mass star-forming regions (see Churchwell 2002 for a review).

Despite significant progress during recent years, the driving mechanism, origin, structure, physical and chemical properties, and dynamics of these massive outflows are poorly understood due to the limitations of available samples studied in detail. There have been only a few systematic studies on massive outflows by mapping CO lines to date (Shepherd & Churchwell 1996b; Ridge & Moore 2001; Beuther et al. 2002b; Wu et al. 2005; Zhang et al. 2005; Kim & Kurtz 2006, hereafter Paper I). A number of issues related to these objects is still debated. For instance, Beuther et al. (2002b) using the CO J=2-1 line maps of 21 massive YSOs at 11″ resolution found that their outflows have stronger collimation than the ones observed by Shepherd & Churchwell (1996b) and Ridge & Moore (2001) with lower (20″−60″) resolution. Moreover they did not found a tight correlation between mass outflow rate and bolometric luminosity of the central (proto)star, which had been believed to exist over the luminosity range 10^0−10^6 $L_\odot$ (see Shepherd & Churchwell 1996b). Therefore massive outflows still demand our attention.

In this study, we present survey results of HCO^+ J=1−0, SiO J=2−1, 22 GHz H_2O maser, and 44 GHz class I CH_3OH maser lines toward 18 massive YSOs. For six of these massive YSOs, we also present CO J=2–1 line maps. Our main scientific goals are to search for new bipolar molecular outflows associated with massive star formation, and to investigate their physical and dynamical properties. The structure of this paper is as follows. We describe the details of the observations in Section 2. The observational results are presented in Section 3. We compare our observations with the previous single-dish observations of molecular outflows both from low- and high-mass YSOs, and comment on the individual sources in Section 4. We summarize our

Corresponding author: K.-T. Kim

Table 1
Source Summary

			l	b	d	$L_{\rm bol}$	Continuum Emission		Maser Emission			
IRAS Name	α(J2000.0)	δ(J2000.0)	(deg)	(deg)	(kpc)	($L_\odot$)	Radio[a]	(Sub)mm	H_2O	CH_3OH[b]	OH	Other Names
05490+2658	05:52:12.9	+26:59:33	182.416	+0.247	2.1	0.3E4	n (13)	y(1)	n(13)	n(13)	n(4)	S242
07299−1651	07:32:09.8	−16:58:16	232.621	+0.995	1.4	0.6E4	UC[c] (15)	y(10)	y(7)	y(15)	y(2)	S302, DG121, RCW7
20081+3122	20:10:09.2	+31:31:34	69.540	−0.976	1.8	1.0E4	UC[c] (11)	y(9)	y(3)	y(14)	y(12)	ON1, OH69.5−1.0
21306+5540	21:32:11.9	+55:53:50	97.530	+3.185	3.7	1.1E4	UC (8)	y(9)	y(6)	n(14)	y(16)	S128N
22308+5812	22:32:44.7	+58:28:09	105.624	+0.338	3.7	2.1E4	C (5)	y(9)	y(6)	n(14)	n(16)	S138
23133+6050	23:15:30.4	+61:07:20	111.611	+0.377	3.1	0.4E4	UC (11)	y(9)	n(16)	n(14)	n(16)	S159

Note. — Units of right ascension are hours, minutes, and seconds, and units of declination are degrees, arcminutes, arcseconds.
[a]UC: UC HII region; C: compact HII region.
[b]6.7 GHz class II CH_3OH maser.
[c]unresolved UCHII.
References. — (1) Beuther et al. 2002a; (2) Cohen et al. 1988; (3) Comoretto et al. 1990; (4) Edris et al. 2007; (5) Fich 1993; (6) Haschick & Ho 1985; (7) Henning et al. 1992; (8) Ho et al. 1981; (9) Hunter et al. 2000; (10) Klein et al. 2005; (11) Kurtz et al. 1994; (12) Nammahachak et al. 2006; (13) Sridharan et al. 2002; (14) Szymczak et al. 2000; (15) Walsh et al. 1998; (16) Wouterloot et al. 1993

main results in Section 5.

2. OBSERVATIONS

2.1. Source Selection

Our sample consists of 6 bright ($L_{\rm bol}$>10^3 $L_\odot$) Infrared Astronomical Satellite (IRAS) point sources that have colors similar to ultracompact HII regions (hereafter UCHIIs, Wood & Churchwell 1989) and are associated with various indicators of star formation, such as H_2O, CH_3OH, OH maser emission, (sub)millimeter continuum emission, and mid-infrared continuum emission sources (Table 1). The sources were selected from three catalogs of massive YSOs (Hunter et al. 2000; Walsh et al. 2001; Sridharan et al. 2002), because they are located in relatively nearby (<4 kpc) and less crowded ($65°<l<235°$) regions of the Galactic plane. Outflow signatures are often confused by multiple cloud components in the same line of sight for sources with $l<50°$ (Zhang et al. 2001). Three of them appear to be massive protostellar candidates since they show no or very weak radio continuum emission (see Table 1). We found high-velocity wings in all the sources by analyzing single sensitive CO J=1−0 spectra taken with the Seoul Radio Astronomy Observatory (SRAO) 6 m telescope[1] in 2001 November. The telescope has a full width at half-maximum (FWHM) of 100″ and a main-beam efficiency ($\eta_{\rm mb}$) of 0.75 at 115 GHz (Koo et al. 2003). A 1024 channel correlator with 50 MHz bandwidth was used as the backend. All the spectra were taken in position switching mode. The system temperature was typically 300 K.

2.2. ARO 12 m Observations

We mapped the 6 massive YSOs in the CO J=2−1 line using the 12 m telescope[2] at Kitt Peak from 2002 March to May. A 256 channel filterbank with 128 MHz bandwidth was used in serial mode, resulting in a velocity resolution of 0.65 km s^{-1}. The system temperature varied between 400 K and 700 K, depending on the weather condition and the elevation of the source. All the sources were mapped in 8″ spacing by position switching mode using the on-the-fly (OTF) observing technique. The maps are about 5′x5′ in size. The reference positions were checked to be free from appreciable (>0.1 K) CO emission. In 2003 January we also performed HCO^+ J=1−0 and SiO v=0 J=2−1 line surveys toward the 6 sources and the 12 massive protostellar candidates studied in Paper I. The typical rms noise levels were about 0.03 and 0.05 K at 86 and 89 GHz, respectively. The pointing was usually checked every 4 hours with planets, and was found to be accurate to within 7″. The observed temperature was obtained on the $T_{\rm R}^*$ scale and was converted to main-beam brightness temperature ($T_{\rm b}$) using $\eta_{\rm mb}^*$. A summary of the observations is presented in Table 2.

2.3. KVN 21 m Observations

We also performed a simultaneous multi-epoch survey of H_2O $6_{16}-5_{23}$ (22.235080 GHz) and class I CH_3OH 7_0-6_1 A^+ (44.069430 GHz) masers toward the 18 massive YSOs. The observations were conducted using the Korean VLBI Network (KVN) 21 m telescopes at the Yonsei (YS) and Ulsan (YS) stations between 2009 June and 2012 December (Kim et al. 2011; Lee et al. 2011). We employed 4096-channel Digital Spectrometers with a bandwidth of 32MHz each. Table 2 gives a summary of the observations. The pointing and focus were checked every 2 hr by observing nearby strong H_2O and SiO maser sources. The pointing accuracy was better than 5″. The data were calibrated by the standard chopper wheel method and the line intensity was obtained on the $T_{\rm A}^*$ scale. The conversion factors between $T_{\rm A}^*$ and the flux density are 11.1 and 11.6 Jy K^{-1} at 22 and 44 GHz, respectively.

All the spectra were taken in the position switching mode with a total (ON+OFF) integration time of 30 minutes, yielding about 0.5 Jy rms noise levels for both transitions at velocity resolutions of 0.21 km s^{-1}. The KVN antennas are shaped Cassegrain type with high (∼14 dB) first sidelobe levels and the first sidelobes are separated by about 1.5 times FWHM from the primary beam center (Kim et al. 2011; Lee et al. 2011). Thus we checked whether the detected maser emission is contaminated by a nearby strong source by making a map of 1.5 FWHM×1.5 FWHM around each source in half-beam spacing. All data were analyzed with the GILDAS/CLASS software.

3. RESULTS

3.1. CO J=2−1 Line Maps

Figures $1a-1f$ show the distributions of blue- and redshifted high-velocity gases in 6 sources of our sample. We identified bipolar outflows in all of them. In four bipolar outflows blue- and redshifted lobes almost overlap (05490+2658, 07299−1651, 20081+3122, 21306+5540). This indicates that the outflows are young and so compact in comparison with the 27″ beam size or that they have wide opening angles but small inclination angles between the outflow axis and the line of sight. We cannot exclude the possibility that they are not single bipolar outflows but combinations of multiple bipolar outflows. Higher-resolution continuum and molecular line studies are required to clarify this issue.

The IRAS point source is located within the beam size to the outflow center in 4 of the identified bipolar outflows (07299−1651, 20081+3122, 21306+5540, 22308+5812). In 22308+5812, the blue- and redshifted lobes are not aligned along a line but inclined nearly perpendicular to each other. We can thus think of at least two other possibilities than that they form a bipolar outflow. One possibility is that two bipolar outflows, i.e., north-south one and east-west one, are entangled around the field center. In this case the IRAS

[1] The SRAO 6 m telescope is operated by Seoul National University with support from the Korea Basic Science Research Institute.

[2] The 12 m telescope is operated by the Arizona Radio Observatory (ARO), Steward Observatory, University of Arizona.

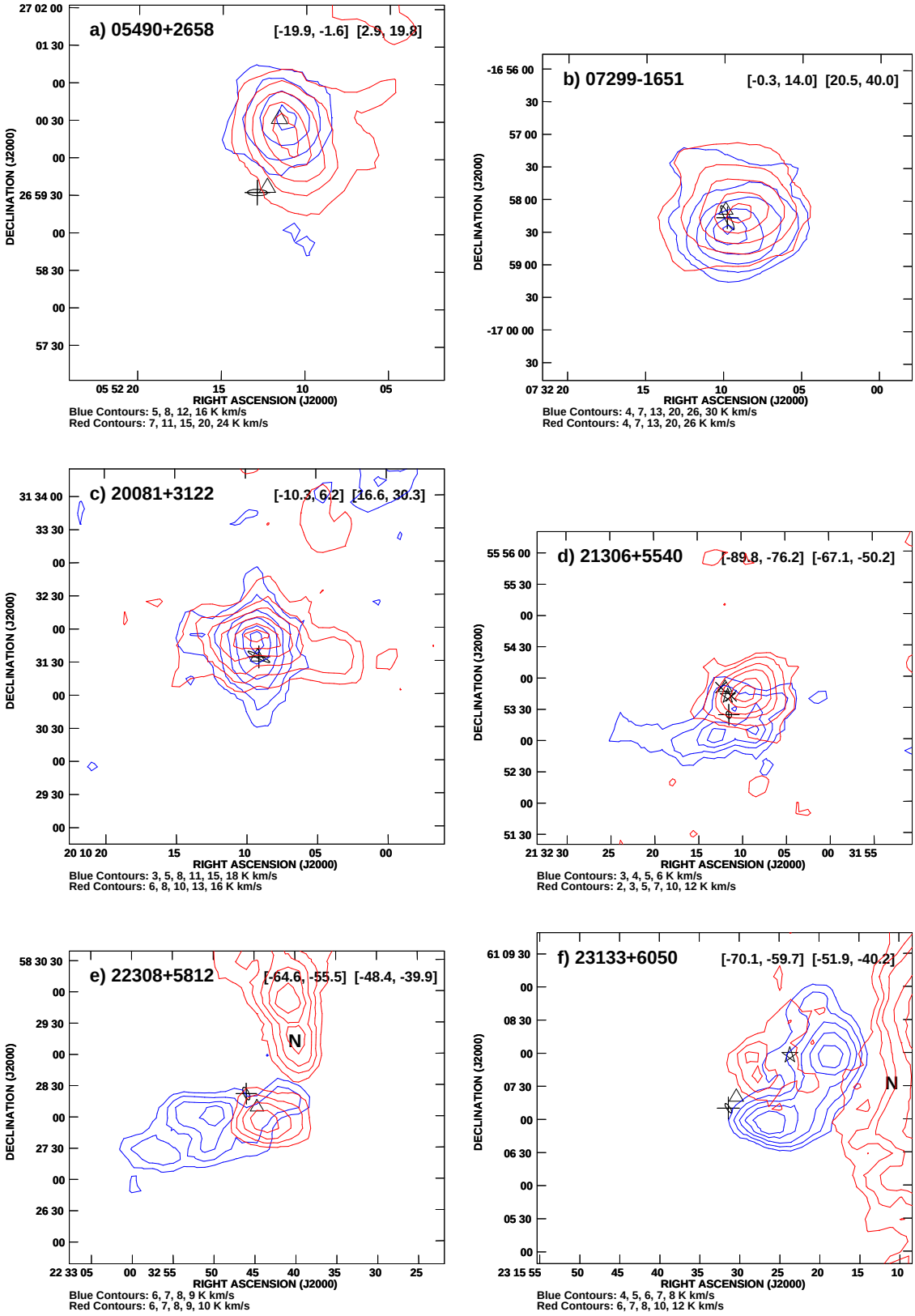

Figure 1. In each panel the blue and red contours show the distributions of blue- and redshifted high-velocity gases, respectively. The integrated velocity ranges are displayed at the top right corner. Each IRAS point source is marked by a cross with the ellipse showing its positional error (1 σ). Triangles indicate (sub)millimeter continuum peaks. Also shown are water masers ($\times$) and radio continuum peaks (*five-pointed star*) *not* associated with the IRAS point sources. All IRAS point sources but 05490+2658 correspond to ultracompact or compact HII regions.

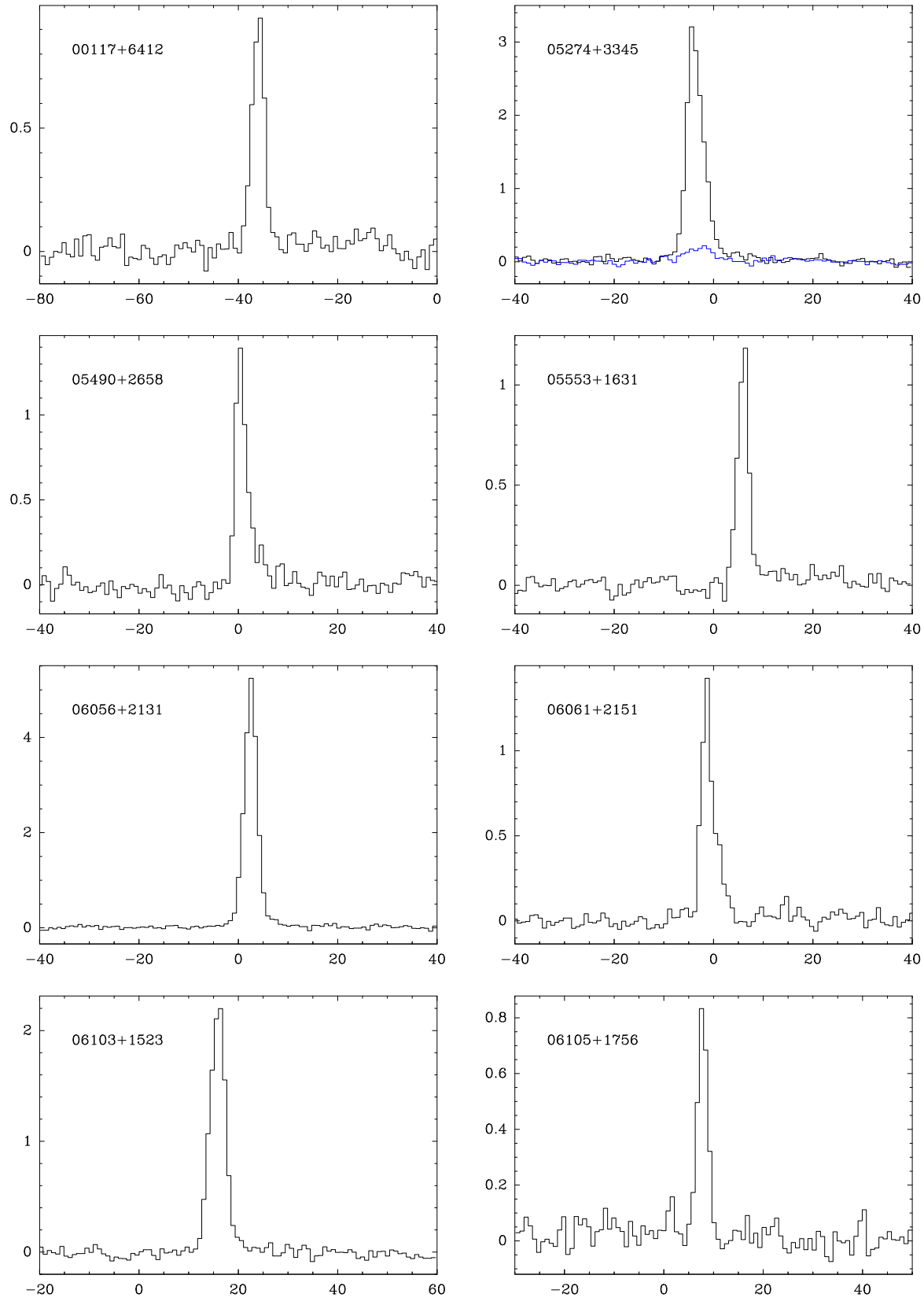

Figure 2. Detected HCO^+ J=1−0 (*black*) and SiO J=2−1 (*blue*) line spectra. The horizontal axis is v_{LSR} in km s^{-1}, while the vertical axis is T_R^* in K. In each panel the *IRAS* source name is presented at the top left corner.

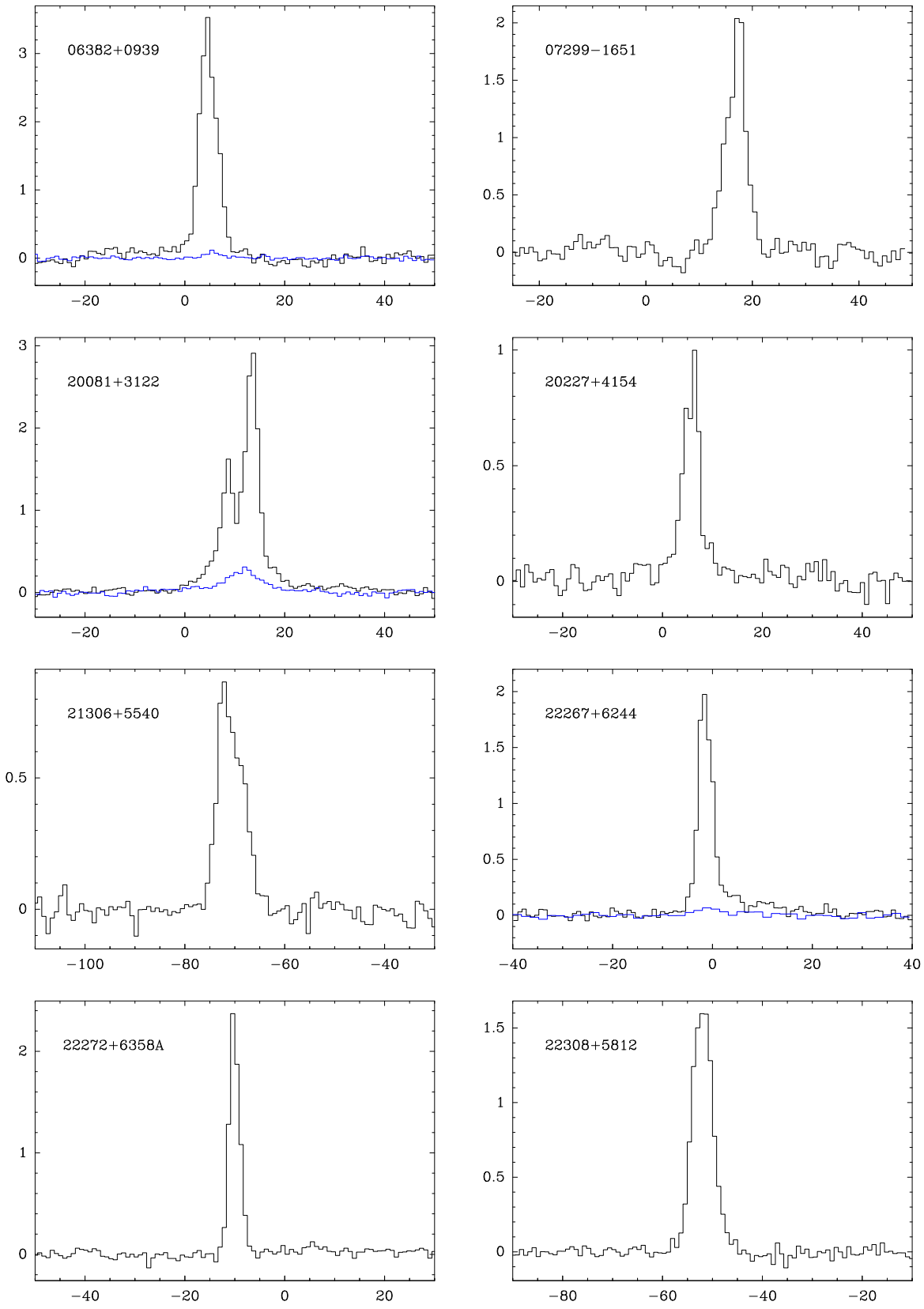

Figure 2. *Continued.*

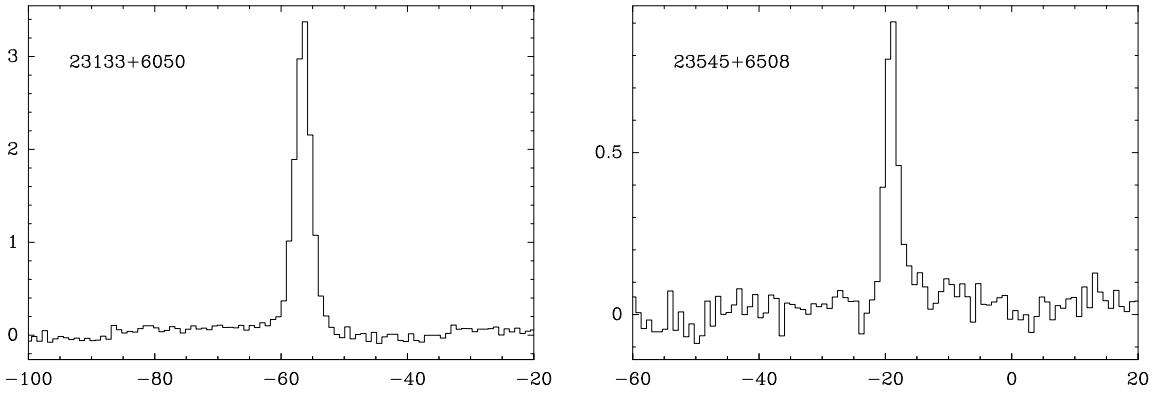

Figure 2. *Continued.*

Table 2
Observational Summary

Telescope and Transition	Frequency (GHz)	Resolution Δf (kHz)	Resolution Δv (km s^{-1})	FWHM ($''$)	$\eta^*_{\rm mb}$ [a]	$\eta_{\rm a}$	$T_{\rm sys}$ (K)
ARO 12-m							
CO J=2−1	230.53800	500	0.65	27	0.51		400−700
HCO^+ J=1−0	89.188518	250	0.84	70	0.90		220
SiO v=0 J=2−1	86.846998	250	0.86	70	0.90		220
KVN 21-m							
H_2O $6_{16}-5_{23}$	22.23508	7.8	0.10	130		0.72	80−150
CH_3OH $7_0-6_1A^+$	44.06943	7.8	0.05	65		0.69	100−200

[a]Corrected main beam efficiency defined as $T_{\rm b}=T^*_{\rm R}/\eta^*_{\rm mb}$.

Table 3
Outflow Properties Derived from CO J=2−1 Line Data

IRAS Name	Size (pc)	$M_{\rm b}$ ($M_\odot$)	$M_{\rm r}$ ($M_\odot$)	$M_{\rm out}$ ($M_\odot$)	P ($M_\odot$ km s^{-1})	E (10^{46}) (erg)	t (10^4) (yr)	$\dot{M}_{\rm out}$ (10^{-4}) ($M_\odot$ yr^{-1})	$F_{\rm m}$ (10^{-3} $M_\odot$) (km s^{-1} yr^{-1})	$L_{\rm m}$ ($L_\odot$)
05490+2658[a]	1.2	9.4	27.6	37.0	665	12.0	6.5	5.7	10.3	14.7
07299−1651[b]	0.9	11.7	11.9	23.6	343	5.0	6.3	3.8	5.5	6.4
20081+3122	1.0	8.5	15.0	23.5	477	9.7	4.8	5.0	10.0	16.2
21306+5540[b]	1.4	14.3	18.2	32.5	404	5.0	11.3	2.9	3.6	3.5
22308+5812[b]	1.9	54.7	19.3	74.0	577	4.6	22.6	3.3	2.6	1.6
23133+6050[b]	0.9	39.3	14.8	54.1	462	4.0	10.5	5.1	4.4	3.0

[a]bipolar outflow for the first time mapped in the CO J=2−1 line
[b]bipolar outflow newly discovered

point source is more likely to be the driving source of the east-west outflow. The other possibility is that the redshifted lobe, especially its northern part, is contaminated by another velocity component. This issue demands further detailed radio and infrared studies. On the other hand, 05490+2658 is significantly offset from the outflow center. This suggests that the IRAS point source may not be the outflow's driving source. The 1.2 mm continuum map of 05490+2658 made by Beuther et al. (2002a) at 11$''$ spatial resolution shows that one of two continuum peaks in the field approximately corresponds to the outflow center. None of H_2O and 6.7 GHz class II CH_3OH masers have been detected (Table 1). This could be in part because the observations were made toward the IRAS point source position rather than the outflow center (see Section 3.4). 23133+6050 also seems to be offset from the outflow center. Lebrón et al. (2001) detected a compact HII region toward the outflow center as well as an UCHII at the position of the IRAS source. The feature at the western boundary of the field does not appear to be high-velocity gas component but another velocity component.

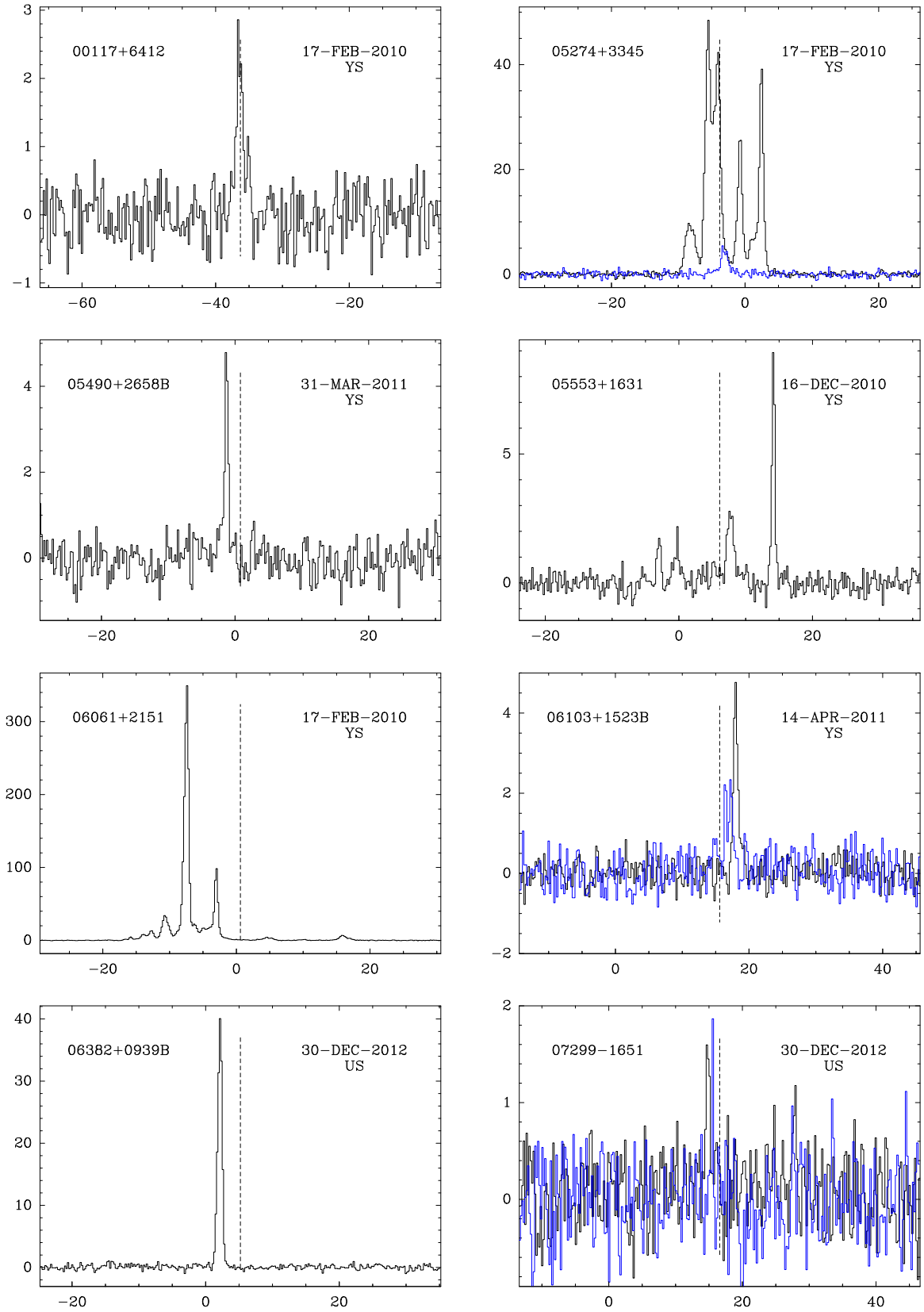

Figure 3. Detected H_2O (*black*) and 44 GHz class I CH_3OH (*blue*) maser spectra. The horizontal axis is v_{LSR} in km s^{-1}, while the vertical axis is flux density in Jy. In each panel the *IRAS* source name is listed at the top left corner while the observing date and KVN station are presented at the top right corner. The vertical dotted line represents the systemic velocity.

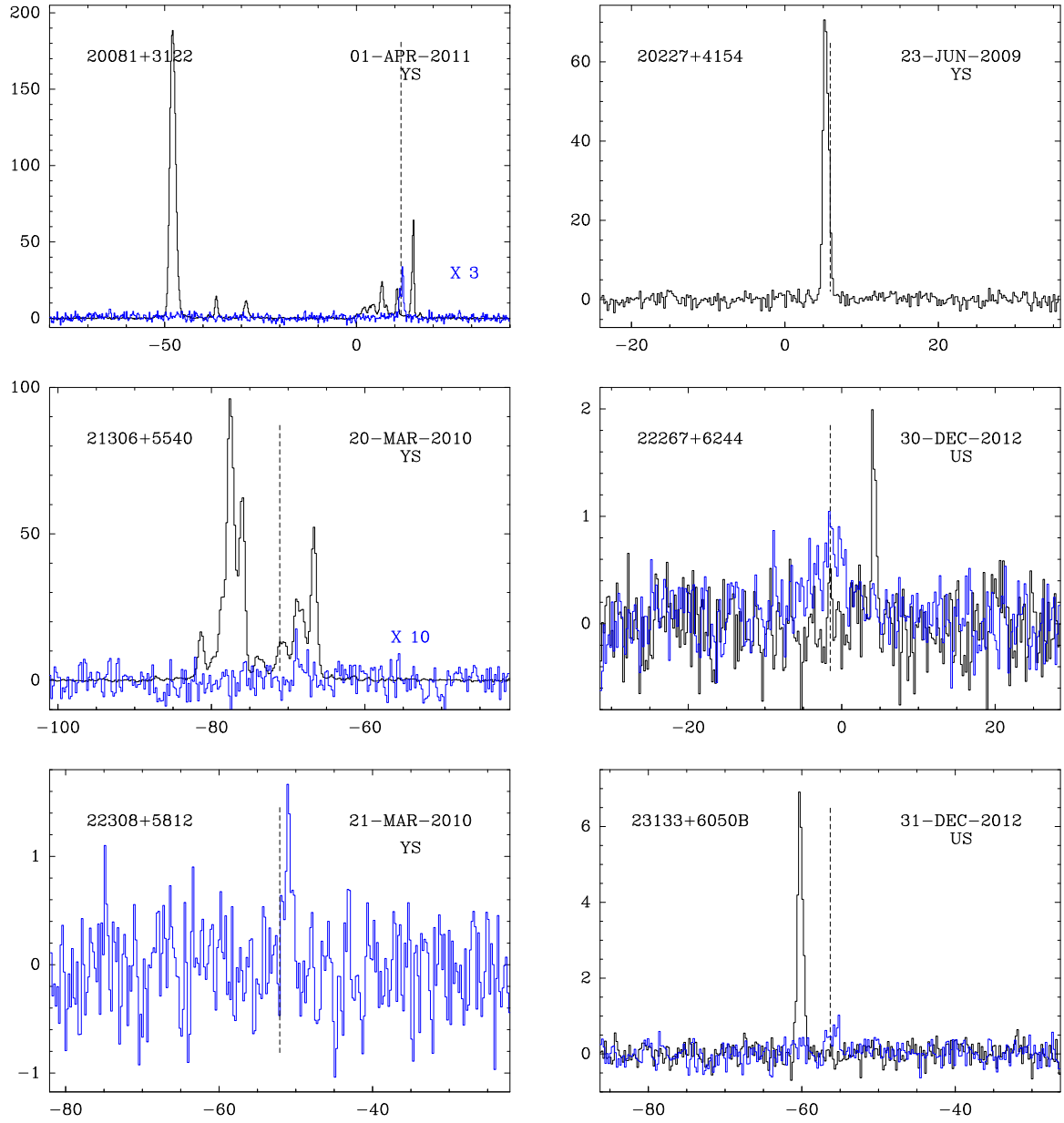

Figure 3. *Continued.*

3.2. Physical and Dynamical Parameters of CO Outflows

The physical and dynamical parameters of the observed outflows were derived in a similar manner to Beuther et al. (2002b) (see also Paper I). Table 3 presents the results: size, masses (blueshifted, redshifted, total), momentum, kinetic energy, dynamical age, mass outflow rate, mechanical force, mechanical luminosity. In this analysis we excluded possibly unrelated components in 22308+5812 and 23133+6050, which are marked by 'N' in Figures 1*e* and 1*f*. We corrected for the opacity of CO J=2−1 line emission, but not for the inclination of the outflows. All outflows have masses >20 $M_\odot$ and momenta >300 $M_\odot$ km s^{-1}. They have dynamical ages of (4−23)×10^4 yr and mass outflow rates of (3−6)×10^{-4} $M_\odot$ yr^{-1}. Therefore these outflows have similar physical and dynamical properties to other outflows from massive YSOs (e.g., Beuther et al. 2002b; Paper I), but have much greater masses, momenta, and outflow rates than outflows from low-mass protostars such as class 0 and class I objects (e.g., Bontemps et al. 1996). The estimated high mass outflow rates suggest high mass accretion rates sufficient to overcome the strong radiation of the central massive (proto)stars (see Section 4 of Paper I).

Table 4
HCO^+ Line Parameters

IRAS Name	v_{sys} (km s^{-1})	v_{LSR} (km s^{-1})	T_R^* (K)	Δv (km s^{-1})	$\int T_R^* dv$ (K km s^{-1})	Line Wing
00117+6412[a]	−36.3	−35.6	1.0	3.4	2.9	n
05274+3345[a]	−3.8	−4.8	3.2	4.2	13.8	Y
05490+2658	0.8	0.4	1.4	2.5	4.7	Y
05553+1631[a]	6.1	6.4	1.2	2.5	3.6	Y
06056+2131[a]	2.6	2.6	5.2	2.5	17.6	Y
06061+2151[a]	−0.6	−1.3	1.4	2.5	4.6	Y
06103+1523[a]	15.6	16.4	2.2	4.2	9.2	n
06105+1756[a]	8.0	7.6	0.8	2.5	2.2	n
06382+0939[a]	5.2	4.6	3.5	4.2	15.3	Y
07299−1651	16.6	17.1	2.0	4.2	9.1	Y
20081+3122[b]	11.6	10.4	2.9	-	18.1	Y
20227+4154[a]	5.9	6.4	1.0	3.4	4.2	Y
21306+5540	−71.1	−72.1	0.9	5.9	5.2	Y
22267+6244[a]	−1.5	−1.6	2.0	3.4	8.7	Y
22272+6358A[a]	−9.9	−10.4	2.4	2.5	6.1	n
22308+5812	−52.1	−52.1	1.6	4.2	8.7	n
23133+6050	−56.3	−56.2	3.4	3.4	11.5	n
23545+6508[a]	−18.4	−18.7	0.9	2.5	2.8	n

[a]The sources of Paper I.
[b]This source has a double-peaked profile. v_{LSR} is the velocity of the central absorption dip, while T_R^* is the red peak temperature. Δv is not determined because the central peak temperature is not unknown due to the self-absorption dip.

Table 5
SiO Line Parameters

IRAS Name	v_{LSR} (km s^{-1})	T_R^* (K)	Δv (km s^{-1})	$\int T_R^* dv$ (K km s^{-1})	N(SiO) (10^{12} cm^{-2})
05274+3345[a]	−1.8	0.2	6.0	1.4	5.2
06382+0939[a]	5.4	0.1	2.6	0.3	1.1
20081+3122	11.1	0.3	-	3.1	11.4
22267+6244[a]	−1.2	0.07	-	0.4	1.5

[a]The sources of Paper I.

3.3. HCO^+ J=1−0 and SiO v=0 J=2−1 Line Surveys

The HCO^+ J=1−0 and SiO v=0 J=2−1 lines were observed toward 18 sources of which 6 and 12 sources were mapped by this study and Paper I in the CO J=2−1, respectively, as noted in Section 2.2. The HCO^+ line emission was detected in all sources (Figure 2, Table 4). The line profiles are single peaks for all but one and are non-Gaussian for many of them. The one exception is 20081+3122, which shows a clear double-peak profile with a stronger red peak. This is very likely to be caused by self-absorption because the optically thin $C^{34}S$ line emission is visible at the central dip (Larionov et al. 1999). We found significant ($\geq 3\sigma$) residual high-velocity gas in 11 (61%) sources, including 20081+3122, after subtracting the fitted single Gaussian. For 20081+3122, we fitted a single Gaussian to the double-peaked profile after masking the absorption dip as in Purcell et al. (2006).

The detection rate (61%) is similar to that of Szymczak et al. (2007), who surveyed the same transition toward 27 massive protostellar candidates that are 6.7 GHz CH_3OH maser sources without associations with OH masers or UCHII candidates, and found high-velocity wings in 17 sources (63%). Their rms noise levels (∼0.05 K) were similar to ours. The sources in our survey are mostly IRAS point sources with infrared colors similar to UCHIIs. Only six of them are associated with 6.7 GHz methanol masers (Table 1; Table 1 of Paper I). They are located in the Galactic longitude (l) range, 60°−240°, while the sources of Szymczak et al. (2007) are located closer to the Galactic center, 20°−40°. Purcell et al. (2006) also surveyed the HCO^+ line toward 83 massive protostellar candidates that are all distributed around the Galactic center, $|l|$<32°. Almost all sources are 6.7 GHz CH_3OH maser sources associated with IRAS point sources with infrared colors similar to UCHIIs. They detected the line emission in all sources except one and identified high-velocity line wings toward 26 sources in a similar manner to this study. The detection rate (32%) is half those of this study and Szymczak et al. (2007). The value might be a lower limit because the HCO^+ profiles of many sources in their sample are complex and it is not straightforward to identify line wings. For example, 16 sources clearly contain blends of two or more components. If they are excluded, the detection rate increases to 39%. Their relatively poor sensitivities (0.1−0.2 K)

Table 6
Line Parameters of Detected Masers

IRAS Name	Maser Species	Observing Date	$v_{\rm p}$ (km s^{-1})	$S_{\rm p}$ (Jy)	$\int S_\nu dv$ (Jy km s^{-1})	$v_{\rm min}$ (km s^{-1})	$v_{\rm max}$ (km s^{-1})	$L_{\rm m}$ ($L_\odot$)
00117+6412[a]	H_2O	17-FEB-2010	−36.63	2.9	3.0	−37.05	−35.16	2.83E-06
05274+3345[a]	H_2O	17-FEB-2010	−5.47	48.4	185.0	−9.69	4.43	1.38E-04
	CH_3OH[c]	17-FEB-2010	−3.36	5.5	5.6	−3.57	−2.30	8.31E-06
05490+2658B[b]	H_2O[c]	31-MAR-2011	−1.37	4.9	3.0	−1.58	−0.95	3.90E-06
05553+1631[a]	H_2O	16-DEC-2010	14.11	8.9	12.2	−3.37	14.53	1.42E-05
06061+2151[a]	H_2O	17-FEB-2010	−7.37	349.3	505.8	−16.85	17.49	5.90E-04
06103+1523B[a,b]	H_2O[c]	14-APR-2011	18.00	4.7	3.0	17.58	18.42	1.80E-05
	CH_3OH[d]	14-APR-2011	17.22	2.3	2.3	16.37	17.43	2.66E-05
06382+0939B[a,b]	H_2O[c]	30-DEC-2012	2.16	40.0	32.4	1.31	2.79	6.04E-06
07299−1651	H_2O	30-DEC-2012	14.68	1.5	3.2	14.68	27.96	1.82E-06
	CH_3OH[c]	30-DEC-2012	15.58	1.9	0.5	15.58	15.58	5.25E-07
20081+3122	H_2O	01-APR-2011	−47.88	188.4	518.9	−52.31	16.79	4.90E-04
	CH_3OH[e]	01-APR-2011	11.97	11.2	9.7	11.12	12.40	1.81E-05
20227+4154[a]	H_2O	23-JUN-2009	5.16	70.6	64.0	4.74	6.21	5.39E-05
21306+5540	H_2O	20-MAR-2010	−77.58	96.1	356.0	−87.27	−55.47	1.42E-03
	CH_3OH[c]	21-MAR-2010	−68.94	1.8	0.5	−68.94	−68.94	4.11E-06
22308+5812	CH_3OH[c]	21-MAR-2010	−51.06	1.7	0.7	−51.06	−50.85	5.20E-06
22267+6244[a]	H_2O[c]	30-DEC-2012	4.00	2.0	0.8	4.00	4.43	6.08E-08
	CH_3OH[c]	30-DEC-2012	−1.63	0.9	1.1	−1.63	−0.35	1.64E-07
23133+6050B[b]	H_2O[c]	31-DEC-2012	−60.32	6.9	5.5	−60.95	−59.47	1.51E-05
	CH_3OH[c]	31-DEC-2012	−55.80	0.8	0.5	−55.80	−55.16	2.99E-06

[a]The sources of Paper I.
[b]The coordinates not of the IRAS sources but of the outflow centers (see the text for details): 05490+2658B (05:52:11.6, +27:00:32), 06103+1523B (06:13:17.2, +15:22:56), 06382+0939B (06:41:08.0, +09:34:30), 23133+6050B (23:15:30.4, +61:07:20).
[c]New detections.
[d]previously detected by Fontani et al. (2010).
[e]previously detected by Haschick et al. (1990).

might also cause the low detection rate.

We detected SiO line emission toward 4 of the 18 sources (Figure 2, Table 5). The detection rate (22%) is significantly lower than 37% of Harju et al. (1998), who performed an SiO v=0 J=2−1 line survey toward a much larger sample of massive YSOs identified mainly by the presence of H_2O and OH masers, with similar sensitivities (0.02−0.05 K) and beam sizes (43″−57″). However, they found that the detection rates are different for sources located in different galactic locations. If we only consider sources that are located in the same galactic longitude range (60°−240°) or in the same galactocentric radius range (8 kpc−12 kpc) as our sources, the detection rate is 20%−26%. This is in agreement with the detection rate of this study.

We estimated the column density of SiO using the equation below, assuming (1) the SiO J=2−1 line is emitted from regions in local thermodynamic equilibrium (LTE), (2) it is optically thin, and (3) the excitation temperature of SiO gas is 30 K as for CO gas.

$$N({\rm SiO}) = 9.6\times10^{10}\, T_{\rm ex}\, \exp(4.2/T_{\rm ex}) \int T_{\rm b} dv \quad ({\rm cm}^{-2}), \tag{1}$$

where $T_{\rm ex}$ is the excitation temperature in K, $T_{\rm b}$ is the brightness temperature in K, and v is the velocity in km s^{-1}. The derived values are (1−12)×10^{12} cm^{-2} (Table 5). From the SiO J=8−7 line survey of 23 massive star-forming regions with molecular outflows and UCHIIs, Klaassen & Wilson (2007) also found that the majority of their sources have SiO column densities of order 10^{12} cm^{-2}. If we adopt a fractional abundance, [SiO]/[H_2], of 1×10^{-10}, the corresponding H_2 column densities are of order 10^{22} cm^{-2}, comparable to the values previously reported for massive star-forming cores (e.g., Minier et al. 2005).

3.4. H_2O and CH_3OH Maser Surveys

We detected 22 GHz H_2O and 44 GHz class I CH_3OH maser emission toward 13 (72%) and 8 (44%) sources, respectively (Table 6). As mentioned in Section 3.1 and Section 3.1 of Paper I, there are 5 cases in which the IRAS sources are significantly offset from the outflow centers. We observed both positions in each of them, and detected H_2O and CH_3OH masers toward the outflow center in 4 of them. Of the detected sources, 7 sources show both masers and 5 H_2O and 6 CH_3OH maser sources are new discoveries (Table 6). Here we compared our results with previous studies of the two masers using the VizieR service (Ochsenbein et al. 2000). Figure 3 shows the detected H_2O and CH_3OH maser spectra. The detection rate of maser emission depends on the observational sensitivity, the number of epochs, and the evolutionary stage of the central object (Furuya et al. 2001; Bae et al. 2011). The detection rates of the two masers in each epoch are roughly comparable to those of larger samples of high-mass protostellar objects with similar detection limits, 40%−50%

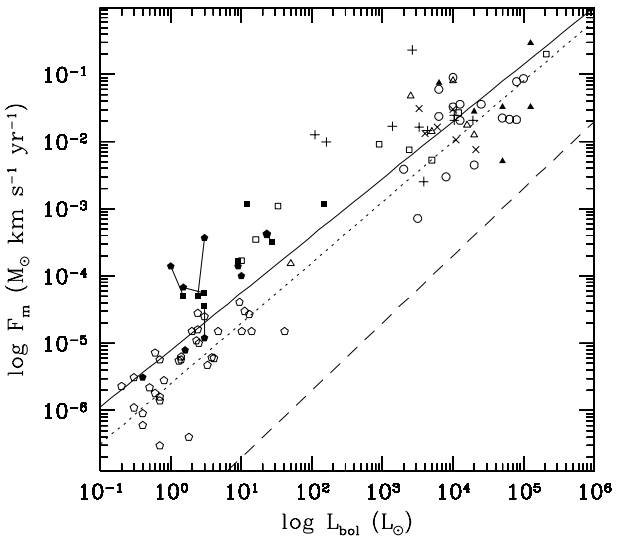

Figure 4. Plot of $F_{\rm m}$ against $L_{\rm bol}$. The tilted crosses indicate the outflows of this study, while the pentagons, squares, circles, and crosses represent the outflows of Bontemps et al. (1996), Cabrit & Bertout (1992), Beuther et al. (2002b), and Paper I, respectively. The solid line is the fitted relation to all data points except for Class 0 objects (*filled pentagons*) of Bontemps et al. (1996). The short solid lines connect the two different measurements of the same sources. See the text for details.

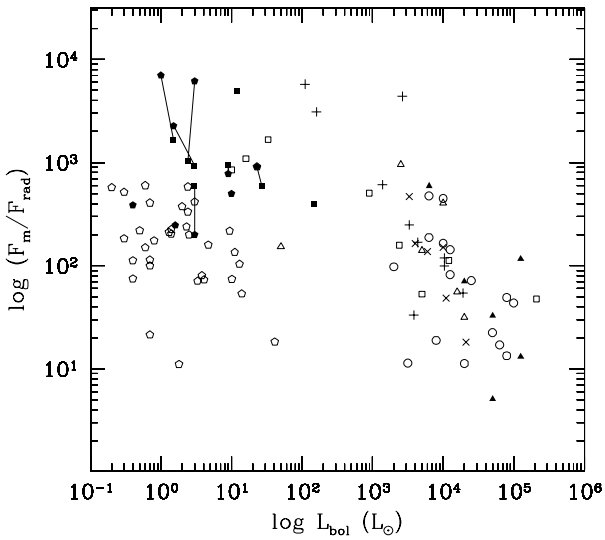

Figure 5. $F_{\rm m}/F_{\rm rad}$ ratio versus $L_{\rm bol}$. The same data sets and symbols as in Figure 4.

for H_2O and ∼30% for 44 GHz CH_3OH (Sridharan et al. 2001; Kang et al. 2015). In contrast, Churchwell et al. (2002) obtained a higher detection rate (67%) of H_2O maser for 84 UCHIIs, which may be more evolved than the sources in our sample, in a single-epoch survey with a comparable flux limit.

The CH_3OH maser spectra show single velocity components around the systemic velocities, $v_{\rm sys}$, which were determined by the CS J=2–1 line observations for the sources in this study (Bronfman et al. 1996) and by the NH_3 (1,1) line observations for the sources in Paper I (Molinari et al. 1996) (Table 4). In contrast, the H_2O maser spectra sometimes exhibit multiple components. Particularly 20081+3122 shows H_2O maser lines that are significantly (>30 km s^{-1}) offset from the systemic velocity. Kurtz & Hofner (2005) also detected these high-velocity features using the Effelsberg 100 m telescope (FWHM=40″), but they were much weaker. These features can be produced by a high-velocity bipolar outflow at a small inclination with the line of sight. Table 6 presents the line parameters of the detected H_2O and CH_3OH masers, including the peak velocity, peak flux density, integrated flux density, and the minimum and maximum values of velocity range. We derived the isotropic luminosities from the integrated flux densities for both masers in the same manner as in Bae et al. (2011). The estimated values are comparable to those of other massive YSOs (e.g., Kang et al. 2015; see also Bae et al. 2011), and are listed in Table 6. One of the scientific goals of this multi-epoch survey is to investigate the time variability of the two masers. The results will be presented in a separate paper.

4. DISCUSSION

4.1. Correlations among CO Outflow Parameters

4.1.1. $L_{\rm bol} - F_{\rm m}$ Relation

Figure 4 shows the mechanical force of the outflow $F_{\rm m}$ against the bolometric luminosity of the central source $L_{\rm bol}$. The data of this study (*tilted cross*) are combined with those of Bontemps et al. (1996) (*pentagon*), Cabrit & Bertout (1992) (*square*), Beuther et al. (2002b) (*circle*), and Paper I (*cross*). Filled squares and pentagons are Class 0 objects, while open symbols are Class I objects. In this analysis we include only data sets that were estimated in a similar way. In order to correct for the inclination effects as in Bontemps et al. (1996), we multiply a factor to the $F_{\rm m}$ values of the other studies except Cabrit & Bertout (1992). We adopt 2.9 for the factor ($\sin i \cos^{-2} i$) assuming a statistical average of random inclinations, 57.°3 (see Section 3.2 of Bontemps et al. 1996). Cabrit & Bertout (1992) corrected for the inclination effects by deriving the inclination angle of each outflow based on the CO map.

There is a strong correlation between $L_{\rm bol}$ and $F_{\rm m}$. Bontemps et al. (1996) also found a good correlation between the two parameters: $\log F_{\rm m} = (0.9\pm0.15) \log L_{\rm bol} - 5.6\pm0.1$ (*dotted line*). Even though their sample consists of 9 Class 0 objects and 36 Class I objects, the correlation was derived only for Class I objects. This was because Class 0 objects have a different distribution from Class I objects, i.e., they have significantly higher $F_{\rm m}$'s than Class I objects for a given $L_{\rm bol}$ due to more efficient driving their outflows. We perform a least-squares fit to all data points except for the Class 0 objects of Bontemps et al. (1996), and obtained the relation: $\log F_{\rm m} = (0.85\pm0.05) \log L_{\rm bol} - 5.12\pm0.12$ (*solid line*). The correlation coefficient is

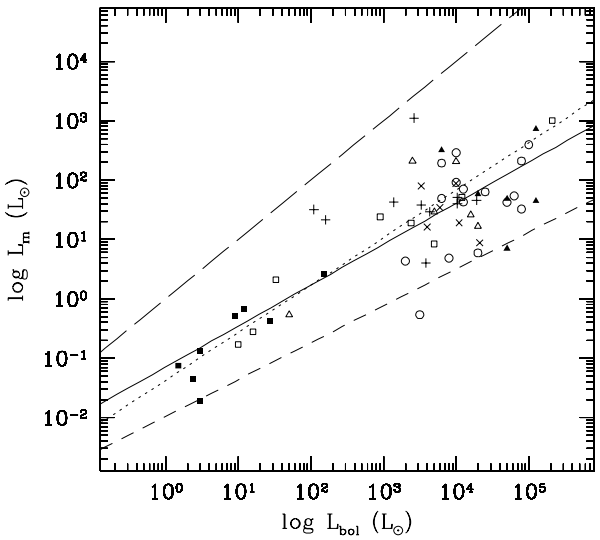

Figure 6. Comparison of $L_{\rm m}$ with $L_{\rm bol}$. The same data sets and symbols as in Figure 4 except Bontemps et al. (1996). The solid line is the relation fitted to all data points, while the dotted and dashed lines show the relations of Cabrit & Bertout (1992) and Wu et al. (2004), respectively.

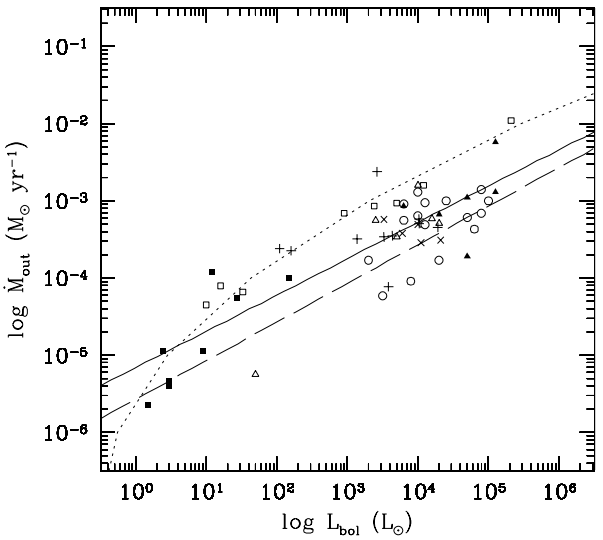

Figure 7. Plot of $\dot{M}_{\rm out}$ versus $L_{\rm bol}$. Symbols are the same as in Figure 4. The solid line shows the linear relation fitted to all data points. The dotted curve and dashed line exhibit the relations derived by Shepherd & Churchwell (1996b) and Wu et al. (2005), respectively.

0.93. The two relations have the same slopes within uncertainties but their y-intercepts are a little different. If we exclude the data of Cabrit & Bertout (1992), we obtain the same relation as Bontemps et al. (1996). Three sources (06382+0939, 20227+4154, 22267+6244) of Paper I have substantially greater $F_{\rm m}$ than the others with similar $L_{\rm bol}$. This suggests that they may be intermediate- or high-mass counterparts of Class 0 objects, which are experiencing active accretion.

The dashed line represents the radiation pressure force $F_{\rm rad}$=$L_{\rm bol}$/c in the case where every stellar photon is absorbed or scattered by the outflow gas *once*. All data points are well above the line. This is consistent with the results of previous studies (e.g., Ridge & Moore 2001) and suggests that the outflows *cannot* be driven by radiation pressure force with single scattering. The difference between $F_{\rm m}$ and $F_{\rm rad}$ tends to reduce as $L_{\rm bol}$ increases. This behavior is more clearly shown in Figure 5 that displays $F_{\rm m}/F_{\rm rad}$ versus $L_{\rm bol}$. The ratios are 100−1000 for most sources at $L_{\rm bol}$<10^4 $L_\odot$, whereas they are lower than 100 for the vast majority of sources with $L_{\rm bol}$>10^4 $L_\odot$. Class 0 objects and the three sources of Paper I mentioned above have on average significantly higher ratios than the other sources.

4.1.2. $L_{\rm bol} - L_{\rm m}$ Relation

Figure 6 shows a plot between $L_{\rm bol}$ and the mechanical luminosity $L_{\rm m}$. The same data sets and symbols are used as in Figures 4 and 5 except Bontemps et al. (1996), which does not provide $L_{\rm m}$. We multiply a correction factor ($\sin i \cos^{-3} i$) of 5.4 to the $L_{\rm m}$ values of this study, Beuther et al. (2002b), and Paper I to correct for a mean inclination angle of 57.°3. We find a quite good correlation between the two parameters. The linear correlation coefficient is 0.83. The solid line is the relation fitted to all data points: log $L_{\rm m}$ = (0.69±0.06) log $L_{\rm bol}$ − 1.15±0.23. The dotted and dashed lines are the relations of Cabrit & Bertout (1992) and of Wu et al. (2004), respectively. The fitted relation is very similar to the Cabrit & Bertout relation. In contrast nearly all data points are distributed above the Wu relation. The scatter is significantly larger in the massive regime than in the low-mass regime. This seems to be reasonable considering both that massive star-forming regions are much more complicated than their low-mass counterparts and that four different data sets are combined in the high-mass regime while just one data set is plotted in the low-mass regime. The long-dashed line represents $L_{\rm m}$=$L_{\rm bol}$. All data points are well below this line.

4.1.3. $L_{\rm bol} - \dot{M}_{\rm out}$ Relation

Figure 7 exhibits the mass outflow rate $\dot{M}_{\rm out}$ versus $L_{\rm bol}$. There appears to be a strong *linear* correlation between the two parameters. A least-squares fit to all data points yields the relation: log $\dot{M}_{\rm out}$ = (0.47±0.04) log $L_{\rm bol}$ − 5.16±0.14 (*solid line*). The correlation coefficient is 0.86. Shepherd & Churchwell (1996b) fitted a second-order polynomial to the data of Cabrit & Bertout (1992) and obtained the relation drawn by the dotted curve: log $L_{\rm bol}$ = 11.2 + 3.35 log $\dot{M}_{\rm out}$ + 0.24 (log $\dot{M}_{\rm out}$)^2. Beuther et al. (2002b) found that almost all data points of their sample are not distributed around the fitted curve but below it, and suggested that the curve might be an upper envelope in the high-mass regime. Most data points of our sample are also located below the curve. The dashed line is the relation fitted to data of more than 200 outflows: log $\dot{M}_{\rm out}$ =

(0.50±0.03) log $L_{\rm bol}$ − 5.57±0.10 (Wu et al. 2005). This line is below our fitted line although the lines have the same slope within uncertainties. This may be because we use data sets corrected for the optical depth and inclination effects, while they used heterogeneous data sets, for many of which those corrections were not available.

4.2. Comments on Individual Sources

4.2.1. IRAS 05490+2658

Snell et al. (1990) mapped this object in the CO J=1–0 line using the Five College Radio Astronomy Observatory (FCRAO) 14 m telescope (FWHM=50″) and detected an unresolved compact bipolar molecular outflow. They also found that the peaks of both lobes roughly overlap and are offset about 60″ northwest from the IRAS point source as in Figure 1*a*. Sridharan et al. (2002) classified this source as a high-mass protostellar object, which is in an earlier evolutionary stage than UCHIIs, based on the lack of radio continuum emission. They observed H_2O and 6.7 GHz class II CH_3OH masers toward the IRAS source, but detected none of them. Beuther et al. (2002a) mapped this field in 1.2 mm continuum emission using the IRAM 30 m telescope (FWHM=11″) and detected two millimeter cores that peak toward the IRAS point source and the outflow center, respectively (Figure 1a, see also Section 3.1). We detected H_2O maser emission only toward the outflow center (Table 6). This is a new detection.

4.2.2. IRAS 07299−1651

Shepherd & Churchwell (1996) made a single-point observation of this source in the CO J=1–0 line using the same telescope (FWHM=60″) as in this study, and detected high-velocity line wings. The full width at zero intensity (FWZI) of the wings was 31.1 km s^{-1}. However, this object has not been mapped in any CO transition to investigate the outflow's properties. Walsh et al. (1998) detected an unresolved UCHII and 6.7 GHz CH_3OH maser emission using the Australia Telescope Compact Array (ATCA).

4.2.3. IRAS 20081+3122

Kurtz et al. (1994) detected an unresolved UCHII toward this object using the Very Large Array (VLA). Xu et al. (2006) mapped this source in the CO J=1–0 line using the Nobeyama Radio Observatory (NRO) 45 m telescope (FWHM=15″) and detected a bipolar outflow. Kumar et al. (2004) also mapped this object in the CO J=2–1 and SiO J=2–1 lines at significantly higher angular resolutions using the IRAM Plateau de Bure Interferometer (PdBI) and claimed to detect four bipolar outflows. The authors cautioned, however, that their maps do not reveal most of the large-scale structures in this region and that the CO data quality was not good because of poor weather condition. This source was for the first time mapped in the CO J=2–1 line using a single-dish telescope in this study.

4.2.4. IRAS 21306+5540

This object was first detected as an UCHII by Ho et al. (1981) using the VLA about 60″ north of a more extended HII region S128, and hence was named as S128N. Shepherd & Churchwell (1996) observed this source in the CO J=1–0 line and detected high-velocity wings (FWZI=33.7 km s^{-1}). There is no previous mapping of this object in any CO line.

4.2.5. IRAS 22308+5812

Fich (1993) detected a compact HII region toward this source using the VLA. There is no previous report about any high-velocity molecular gas or bipolar outflow.

4.2.6. IRAS 23133+6050

Kurtz et al. (1994) detected an UCHII toward this source. As noted in Section 3.1, Lebrón et al. (2001) detected a compact HII region toward the outflow center as well as the UCHII. Thus the outflow could be driven by the ionizing star(s) of the compact HII region. Wu et al. (2005) also mapped this object in the same transition at 29″ grid spacing using the same telescope as in this study four years earlier, but they did not detect any localized structure of high-velocity gas. This might be due to lower sensitivity and/or poor sampling of their observations.

5. CONCLUSIONS AND SUMMARY

We mapped six newly-formed massive stars in the CO J=2–1 line at 27″ angular resolution, and performed surveys of the HCO^+ J=1−0, SiO J=2−1, 22 GHz H_2O maser, and 44 GHz class I CH_3OH maser lines toward the six and twelve other massive YSOs studied in Paper I. The main results in this study are summarized as follows.

1. We detected CO bipolar outflows in all the six sources. Four (07299−1651, 21306+5540, 22308+5812, 23133+6050) of the outflows were newly discovered, while 05490+2658 was for the first time mapped in the CO J=2–1 line. The detected outflows are much more massive and energetic than outflows from low-mass YSOs: masses >20 $M_\odot$ and momenta >300 $M_\odot$ km s^{-1}. They have mass outflow rates $\gtrsim 3\times10^{-4}$ $M_\odot$ yr^{-1}, which are at least one order of magnitude higher than observed in low-mass YSOs.

2. We detected the HCO^+ J=1−0 line emission in all 18 sources. The HCO^+ spectra show high-velocity wings in 11 (61%) sources. We also detected the SiO J=2−1 line emission in 4 (22%) sources. The estimated column densities of SiO molecules are $(1-12)\times10^{12}$ cm^{-2}.

3. We detected 22 GHz H_2O and 44 GHz class I CH_3OH maser emission in 13 (72%) sources and 8 (44%) sources, respectively. Of the detected sources, 5 H_2O and 6 CH_3OH maser sources are new discoveries. 20081+3122 shows high-velocity H_2O maser lines, which can be generated by an outflow with small inclination to the line of sight.

4. We combined the outflow parameters of this study with those of previous studies of both low- and high-mass YSOs, and obtained good correlations of $L_{\rm bol}$ with $F_{\rm m}$, $L_{\rm m}$, and $\dot{M}_{\rm out}$. In the $L_{\rm bol}-F_{\rm m}$ plot we identified 3 intermediate- or high-mass counterparts of Class O objects: 06382+0939, 20227+4154, 22267+6244.

Acknowledgments

We thank H. Beuther for providing the revised parameter values of their sample. We are also grateful to all staff members in the KVN who helped to operate the array. The KVN is a facility operated by the Korea Astronomy and Space Science Institute.

References

Bachiller, R. 1996, Bipolar Molecular Outflows from Young Stars and Protostars, ARA&A, 34, 111

Bae, J.-H., Kim, K.-T., Youn, S.-Y., et al. 2011, A Multi-Epoch, Simultaneous Water and Methanol Maser Survey toward Intermediate-Mass Young Stellar Objects, ApJS, 196, 21

Beuther, H., Schilke, P., Menten, K. M., et al. 2002a, High-Mass Protostellar Candidates. II. Density Structure from Dust Continuum and CS Emission, ApJ, 566, 945

Beuther, H., Schilke, P., Sridharan, T. K., et al. 2002b, Massive Molecular Outflows, A&A, 383, 892

Bontemps, S., Andre, P., Terebey, S., et al. 1996, Evolution of Outflow Activity around Low-Mass Embedded Young Stellar Objects, A&A, 311, 858

Bronfman, L., Nyman, L.-A., & May, J. 1996, A CS (2–1) Survey of IRAS Point Sources with Color Characteristics of Ultra-Compact HII Regions, A&AS, 115, 81

Cabrit, S., & Bertout, C. 1992, CO Line Formation in Bipolar Flows. III - The Energetics of Molecular Flows and Ionized Winds, A&A, 261, 274

Cohen, R. J., Baart, E. E., & Jonas, J. L. 1988, OH Masers Associated wth IRAS Far-Infrared Sources, MNRAS, 231, 205

Comoretto, G., Palagi, F., Cesaroni, R., et al. 1990, The Arcetri Atlas of H2O Maser Sources, A&AS, 84, 179

Churchwell, E. 2002, Ultra-Compact HII Regions and Massive Star Formation, ARA&A, 40, 27

Churchwell, E., Walmsley, C. M., & Cesaroni, R. 1990, A Survey of Ammonia and Water Vapor Emission from Ultracompact HII Regions, A&AS, 83, 119

Edris, K. A., Fuller, G. A., & Cohen, R. J. 2007, A Survey of OH Masers towards High Mass Protostellar Objects, A&A, 465, 865

Fich, M. 1993, A VLA Survey of Optically Visible Galactic H II Regions, ApJS, 86, 475

Fontani, F., Cesaroni, R., & Furuya, R. S. 2010, Class I and Class II Methanol Masers in High-Mass Star-Forming Regions, A&A, 517, 56

Furuya, R. S., Kitamura, Y., Wootten, H. A., et al. 2001, Water Maser Survey toward Low-Mass Young Stellar Objects in the Northern Sky: Observational Constraints on Maser Excitation Conditions, ApJ, 559, L143

Harju, J., Lehtinen, K., Booth, R. S., et al. 1998, A Survey of SiO Emission towards Interstellar Masers. I. SiO Line Characteristics, A&AS, 132, 211

Haschick, A. D., & Ho, P. T. P. 1985, Formation of OB Clusters – CO, NH3, and H2O Observations of the Distant H II Region Complex in S128, ApJ, 292, 200

Haschick, A. D., Menten, K. M., & Baan, W. A. 1990, Detection of Widespread Strong Methanol Masers at 44 GHz, ApJ, 345, 556

Henning, T., Cesaroni, R., Walmsley, M., et al. 1992, Maser Search towards Young Stellar Objects, A&AS, 93, 525

Ho, P. T. P., Haschick, A. D., & Israel, F. P. 1981, OB Star Formation in the S128 Region, ApJ, 243, 526

Hunter, T. R., Churchwell, E., Watson, C., et al. 2000, 350 μm Images of Massive Star Formation Regions, AJ, 119, 2711

Kang, H., Kim, K.-T., Byun, D.-Y., et al. 2015, Simultaneous Observation of Water and Class I Methanol Masers toward Class II Methanol Maser Sources, ApJS, 221, 6

Kim, K.-T., Byun, D.-Y., Je, D.-H., et al. 2011, 100-GHz Band Test Observations of the KVN 21-m Radio Telescopes, JKAS, 44, 8

Kim, K.-T., & Kurtz, S. E. 2006, Occurrence Frequency of CO Outflows in Massive Protostellar Candidates, ApJ, 643, 978

Klaassen, P. D., & Wilson, C. D. 2007, Outflow and Infall in a Sample of Massive Star-Forming Regions, ApJ, 663, 1092

Klein, R., Posselt, B., Schreyer, K., et al. 2005, A Millimeter Continuum Survey for Massive Protoclusters in the Outer Galaxy, ApJS, 161, 361

Koo, B.-C., Park, Y.-S., Hong, S. S., et al. 2003, Performance of the SRAO 6-Meter Radio Telescope, JKAS, 36, 43

Kumar, M. S. N., Tafalla, M., & Bachiller, R. 2004, The Structure of the Onsala 1 Star Forming Region, A&A, 426, 195

Kurtz, S., Churchwell, E., & Wood, D. O. S. 1994, Ultracompact H II Regions. 2: New High-Resolution Radio Images, ApJS, 91, 659

Kurtz, S., & Hofner, P. 2005, Water Masers Toward Ultracompact H II Regions, AJ, 130, 711

Larionov, G. M., Val'tts, I. E., Winnberg, A., et al. 1999, Survey of Bipolar Outflows and Methanol Masers in the $C^{32}S$ (2–1) and $CC^{34}S$ (2–1) Lines in the Northern Sky, A&AS, 139, 257

Lebrón, M. E., Rodríguez, L. F., & Lizano, S. 2001, Observations of the Ionized, Neutral, and Molecular Components Associated with an Expanding H II Region, ApJ, 560, 806

Lee, S.-S., Byun, D.-Y., Oh, C.-S., et al. 2011, Single-Dish Performance of KVN 21 m Radio Telescopes: Simultaneous Observations at 22 and 43 GHz, PASP, 123, 1398

Minier, V., Burton, M. G., Hill, T., et al. 2005, Star-Forming Protoclusters Associated with Methanol Masers, A&A, 429, 945

Molinari, S., Brand, J., Cesaroni, R., et al. 1996, A Search for Precursors of Ultracompact HII Regions in a Sample of Luminous IRAS Sources. I. Association with Ammonia Cores, A&A, 308, 573

Nammahachak, S., Asanok, K., Hutawarakorn K. B., et al. 2006, OH Masers Associated with Bipolar Outflow in ON1, MNRAS, 371, 619

Ochsenbein, F., Bauer, P., & Marcout, J. 2000, The VizieR Database of Astronomical Catalogues, A&AS, 143, 23

Osterloh, M., Henning, T., & Launhardt, R. 1997, Infrared Images and Millimeter Data from Cold Southern IRAS Sources, ApJS, 110, 71

Purcell, C. R., Balasubramanyam, R., Burton, M. G., et al. 2006, A CH_3CN and HCO^+ Survey towards Southern Methanol Masers Associated with Star Formation, MN-

RAS, 367, 553
Ridge, N. A., & Moore, T. J. T. 2001, A Single Distance Sample of Molecular Outflows from High-Mass Young Stellar Objects, MNRAS, 378, 495
Shepherd, D. S., & Churchwell, E. 1996a, High-Velocity Molecular Gas from High-Mass Star Formation Regions, ApJ, 457, 267
Shepherd, D. S., & Churchwell, E. 1996b, Bipolar Molecular Outflows in Massive Star Formation Regions, ApJ, 472, 225
Snell, R. L., Dickman, R. L., & Huang, Y.-L. 1990, Molecular Outflows Associated with a Flux-Limited Sample of Bright Far-Infrared Sources, ApJ, 352, 139
Sridharan, T. K., Beuther, H., Schilke, P., et al. 2002, High-Mass Protostellar Candidates. I. The Sample and Initial Results, ApJ, 566, 931
Szymczak, M., Hrynek, G., & Kus, A. J. 2000, A Survey of the 6.7 GHz Methanol Maser Emission from IRAS Sources. I. Data, A&AS, 143, 269
Szymczak, M., Bartkiewicz, A., & Richards, A. M. S. 2007, A Multi-Transition Molecular Line Study of Candidate Massive Young Stellar Objects Associated with Methanol Masers, A&A, 468, 617
Walsh, A. J., Burton, M. G., Hyland, A. R., et al. 1998, Studies of Ultracompact HII Regions – II. High-Resolution Radio Continuum and Methanol Maser Survey, MNRAS, 301, 640
Walsh, A. J., Bertoldi, F., Burton, M. G., et al. 2001, Mid-Infrared Observations of Methanol Maser Sites and Ultracompact H ii Regions: Signposts of High-Mass Star Formation, MNRAS, 326, 36
Wood, D. O. S., & Churchwell, E. 1989, Massive Stars Embedded in Molecular Clouds – Their Population and Distribution in the Galaxy, ApJ, 340, 265
Wouterloot, J. G. A., Brand, J., & Fiegle, K. 1993, IRAS Sources beyond the Solar Circle. III - Observations of H_2O, OH, CH_3OH and CO, A&AS, 98, 589
Wu, Y., Wei, Y., Zhao, M., et al. 2004, A Study of High Velocity Molecular Outflows with an Up-to-Date Sample, A&A, 426, 503
Wu, Y., Zhang, Q., Chen, H., et al. 2005, CO J = 2-1 Maps of Bipolar Outflows in Massive Star-Forming Regions, AJ, 129, 330
Xu, Y., Shen, Z.-Q., Yang, J., et al. 2006, Molecular Outflows around High-Mass Young Stellar Objects, AJ, 132, 20
Zhang, Q., Hunter, T. R., Brand, J., et al. 2001, Search for CO Outflows toward a Sample of 69 High-Mass Protostellar Candidates: Frequency of Occurrence, ApJ, 552, L167
Zhang, Q., Hunter, T. R., Brand, J., et al. 2005, Search for CO Outflows toward a Sample of 69 High-Mass Protostellar Candidates. II. Outflow Properties, ApJ, 625, 864